Li, Zhen; Hu, Jianke; Han, Yifeng; Li, Hefeng; Wang, Jun; Lund, Peter

Parameter identification and generality analysis of photovoltaic module dual-diode model based on artificial hummingbird algorithm

Published in:
Clean Energy

DOI:
10.1093/ce/zkad066

Published: 01/12/2023

Document Version
Publisher's PDF, also known as Version of record

Please cite the original version:
Li, Z., Hu, J., Han, Y., Li, H., Wang, J., & Lund, P. (2023). Parameter identification and generality analysis of photovoltaic module dual-diode model based on artificial hummingbird algorithm. *Clean Energy*, *7*(6), 1219–1232. https://doi.org/10.1093/ce/zkad066

Clean Energy, 2023, Vol. 7, No. 6, 1219–1232
https://doi.org/10.1093/ce/zkad066
Advance access publication 17 November 2023
Research Article

Parameter identification and generality analysis of photovoltaic module dual-diode model based on artificial hummingbird algorithm

Zhen Li[1], Jianke Hu[2], Yifeng Han[2], Hefeng Li[1], Jun Wang[1,*], and Peter D. Lund[1,3,*]

[1]Jiangsu Provincial Key Laboratory of Solar Energy Science and Technology, School of Energy & Environment, Southeast University, Nanjing 210096, China
[2]PowerChina Huadong Engineering Corporation Limited, No. 201 Gaojiao Road, Hangzhou 311122, China
[3]School of Science, Aalto University, FI-00076, Aalto(Espoo), Finland
[*]Corresponding authors. E-mail: 101010980@seu.edu.cn (J. Wang); peter.lund@aalto.fi (P.D. Lund)

Abstract

The aim of this study is to propose a photovoltaic (PV) module simulation model with high accuracy under practical working conditions and strong applicability in the engineering field to meet various PV system simulation needs. Unlike previous model-building methods, this study combines the advantages of analytical and metaheuristic algorithms. First, the applicability of various metaheuristic algorithms is comprehensively compared and the seven parameters of the PV cell under standard test conditions are extracted using the double diode model, which verifies that the artificial hummingbird algorithm has higher accuracy than other algorithms. Then, the seven parameters under different conditions are corrected using the analytical method. In terms of the correction method, the ideal factor correction is added on the basis of previous methods to solve the deviation between simulated data and measured data in the non-linear section. Finally, the root mean squared error between the simulated current data and the measured current data of the proposed model under three different temperatures and irradiance is 0.0697, 0.0570 and 0.0289 A, respectively.

Received: 7 June 2023. **Accepted:** 6 August 2023

Graphical Abstract

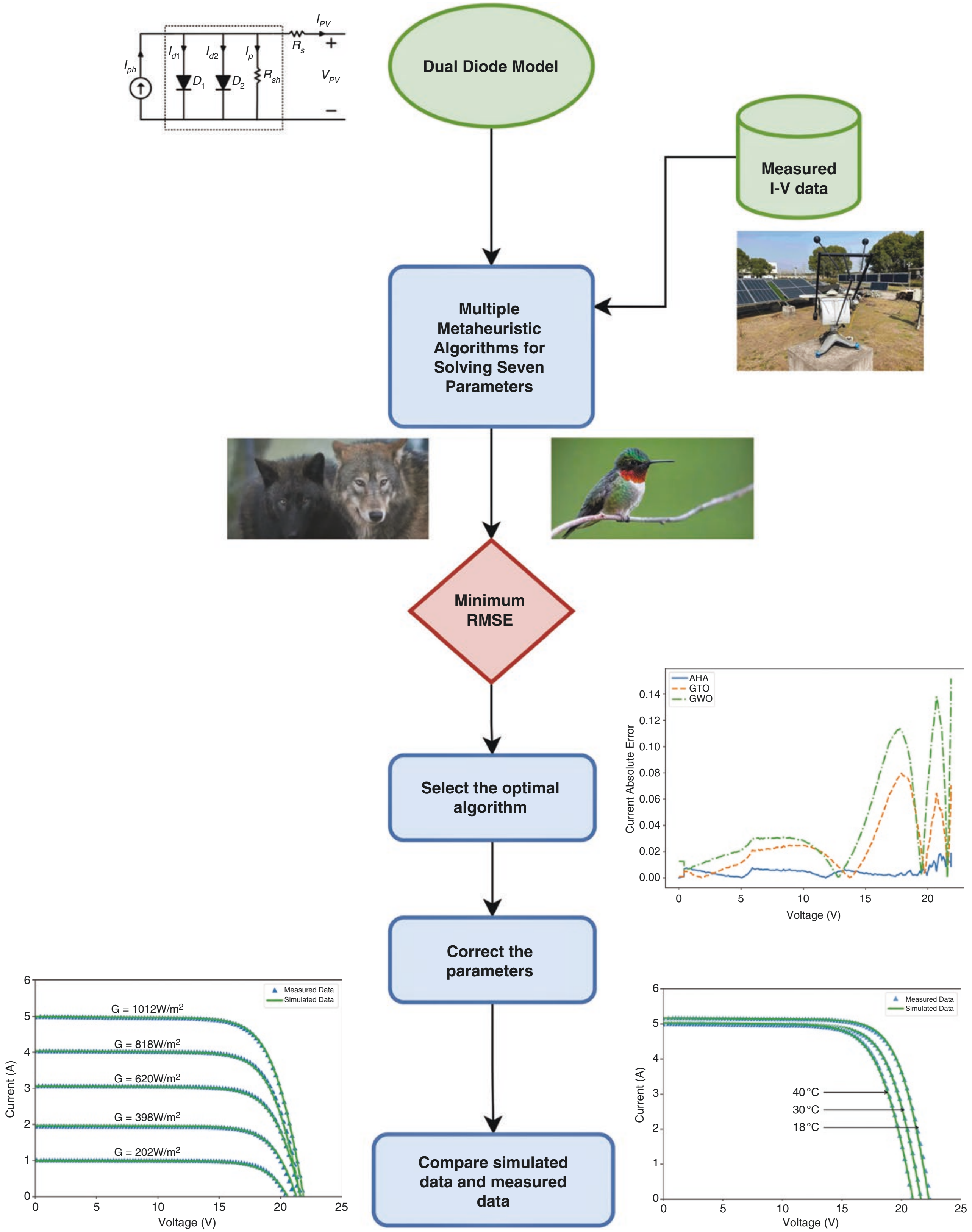

Keywords: photovoltaic modules; dual-diode model; parameter identification; metaheuristic algorithms; parameter correction

Introduction

Accurate modelling is essential for photovoltaic (PV) systems. Over the past few decades, significant progress has been made in understanding the behaviour of these systems through mathematical modelling. Widely used models simulate actual PV cells by fitting the current–voltage data (*I–V*) measured under all operating conditions [1].

In the literature, there are mainly two types of PV cell and module models: the single-diode [2–7] and double-diode (DD) [8–13] models. These equivalent models require estimation of five and seven parameters, respectively. Accurate extraction of PV cell model parameters is crucial not only to evaluate their performance but also to improve design, optimizing manufacturing processes and quality control [14]. Therefore, there is an urgent need for feasible parameter identification techniques.

The methods and steps for parameter extraction of the single- and double-diode models are essentially the same, with the only difference being the number of model parameters. However, multiple studies have shown that the single-diode model neglects recombination losses in the space-charge region, while the DD model can more accurately reflect the behaviour of solar panels [15–18], particularly at low irradiance levels [19]. Therefore, this study adopts the DD model for parameter extraction.

The non-linear, multivariate and multimodal characteristics of PV models make parameter extraction a challenging and significant task. In recent years, various methods have been proposed for parameter extraction of PV models, which can be broadly classified into two categories: key-point-based methods and *I–V* characteristic curve-based methods [20].

The key-point-based method is a commonly used analytical method that simulates the extraction of parameters from the *I–V* curve by using three key points of the manufacturer's catalogue *I–V* curve. The authors have simplified some aspects of this method to reduce the number of unknown parameters or make some approximations. However, this method is largely based on the correctness of several key points on the *I–V* curve, such as the open-circuit voltage, short-circuit current, the maximum power current and the maximum power voltage [21–24]. Essentially, the analytical method summarizes all measured *I–V* data using selected points. If these selected points are assigned incorrectly, the error in parameter extraction can be significant. Therefore, although the analytical method is convenient to use, it often produces uncertain and unsatisfactory results, requiring a large amount of computation, complex mathematical operations and significant time and cost [25].

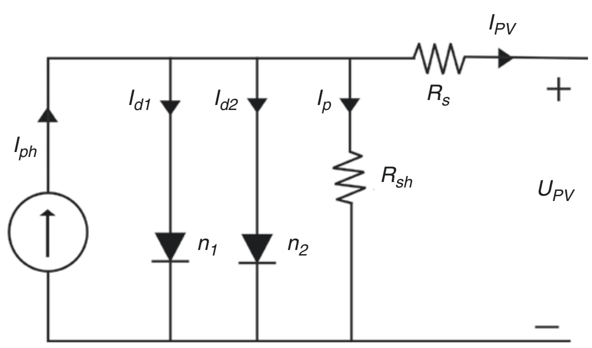

Fig. 1: Equivalent circuit to the DD model

The *I–V* characteristic curve-based method for PV cell parameter identification is currently popular and involves the use of metaheuristic algorithms, which are global optimization techniques based on population iteration. These algorithms can solve various complex problems, particularly complex and highly non-linear optimization problems [26, 27]. One of their most critical advantages is that they do not require an exact mathematical model of the system under study [28], thus significantly reducing the computational burden. Many metaheuristic algorithms have been reported to be remarkably fast for identifying PV cell parameters, including the genetic algorithm (GA) [29, 30], particle swarm optimization (PSO) [31–33], the whale optimization algorithm (WOA) [34], the differential evolution algorithm (DE) [34–36], the sine–cosine algorithm (SCA) [37] and others. These methods utilize basic formulas to solve parameters and utilize all data points more comprehensively while avoiding mathematical complexity. However, optimal performance still requires a reasonable setting of population size, search range and search strategy. As metaheuristic algorithms continue to evolve, better-performing ones are proposed for solving multimodal optimization problems, such as the improved grey wolf optimizer (IGWO) [38], white shark optimizer (WSO) [39], artificial hummingbird algorithm (AHA) [40] and others.

The main challenge with metaheuristic algorithms lies in the algorithms themselves, as their convergence depends on random and heuristic search strategies [41]. Additionally, since the extraction of PV model parameters is a complex multimodal optimization problem, it requires more robust metaheuristic algorithms. As a result, researchers are continually working to develop more accurate, reliable and efficient metaheuristic algorithms for solar PV cell model parameter extraction. This is an ongoing process that requires constant exploration and improvement to meet the growing demand for renewable energy.

However, while utilizing the aforementioned heuristic algorithms to compute PV cell parameters, they commonly acquire parameters solely from *I–V* characteristic curves that were measured under varying conditions. The objective is to confirm that the *I–V* characteristic curve, simulated by utilizing parameters that were acquired through the newly proposed algorithm, is more closely aligned with the experimental data than when utilizing other algorithms [42–44]. However, the extracted parameters are only mathematical abstractions, lacking actual physical meanings.

Within practical engineering applications, we strive to utilize scarce data to simulate data that are boundless. This has been acknowledged within analytical approaches, in which parameters under reference conditions are acquired by formulating and streamlining equations [6,16,43,44]. However, for PV cell output characteristics under different conditions, the acquired parameters are commonly adjusted under actual operating conditions. However, the analytical approach itself condenses all measured *I–V* data via selected points, thereby presenting some uncertainties.

After thoroughly weighing the merits and demerits of these two approaches, our research used all data points on the *I–V* characteristic curve under reference conditions. We utilized the latest metaheuristic algorithm, which has demonstrated remarkable efficacy in engineering quandaries, to extract seven parameters. Additionally, we introduced a novel modification methodology for the seven parameters within analytical approaches that was applicable to metaheuristic algorithms. This approach serves to verify the margin of error between the simulated data and the

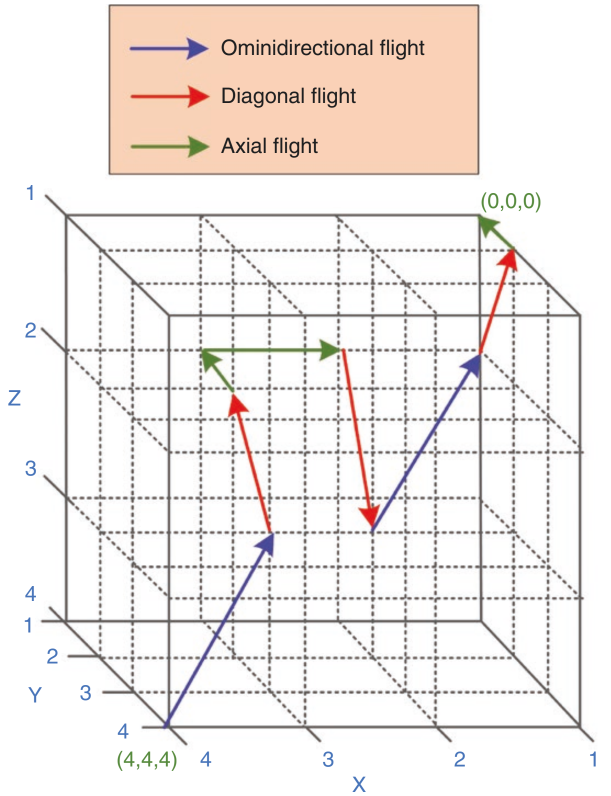

Fig. 2: Three flight behaviours in 3D space

measured data under different conditions, such as temperature and irradiance.

1 PV models and problem formulation

1.1 Solar cells

The DD model has been widely used to simulate the characteristics of solar cells. The equivalent circuit of the DD model is shown in Fig. 1.

Based on the Shockley equation, in the DD model, the output current is calculated as follows [45, 46]:

$$\begin{aligned} I_{PV} &= I_{ph} - I_{d1} - I_{d2} - I_p \\ &= I_{ph} - I_{o1}\left\{\exp\left[\tfrac{q(U_{PV}+I_{PV}R_s)}{n_1kT}\right]-1\right\} - \\ &\quad I_{o2}\left\{\exp\left[\tfrac{q(U_{PV}+I_{PV}R_s)}{n_2kT}\right]-1\right\} - \tfrac{U_{PV}+I_{PV}R_s}{R_{sh}} \end{aligned} \quad (1)$$

where I_{PV} represents the output current, I_{ph} denotes the photo-generated current, I_{d1} and I_{d2} represent the first and second diode currents, I_p denotes the shunt resistor current, I_{o1} and I_{o2} are the saturation and diffusion currents, U_{PV} represents the output voltage, R_s represents the series resistance, $q = 1.60217646 \times 10^{-19}$ C denotes the electron charge, n_1 and n_2 represent the recombination and diffusion diode ideality constants, R_{sh} represents the shunt resistance, T is the cell temperature in Kelvin and $k = 1.380653 \times 10^{-23}$ J/K is the Boltzmann constant.

Equation (1) is the fundamental mathematical expression for PV cells, which describes the relationship between internal parameters and output characteristics. However, calculating the precise values of the parameters (I_{ph}, I_{o1}, I_{o2}, R_s, R_{sh}, n_1, n_2) within the equation is challenging since they are closely tied to the intensity of illumination and the temperature of the solar panel.

1.2 Model of PV panel module

PV modules are composed of a certain number of PV cells connected in series and/or parallel. The parameter extraction method for PV modules essentially breaks down the modules into individual PV cells by their series–parallel connections for analysis. Therefore, in this study, the measurement data for the PV module was transformed into those of a single PV cell using a series–parallel form. We employed the DD model based on PV cells to calculate the seven parameters, which were subsequently substituted into Equation (2), the expression for the output current of the PV module [45, 46]:

$$\begin{aligned} I_{PV}/N_p &= I_{ph} - I_{o1}\left\{\exp\left[\tfrac{q(U_{PV}/N_s+I_{PV}R_s/N_p)}{n_1kT}\right]-1\right\} - \\ & I_{o2}\left\{\exp\left[\tfrac{q(U_{PV}/N_s+I_{PV}R_s/N_p)}{n_2kT}\right]-1\right\} - \tfrac{U_{PV}/N_s+I_{PV}R_s/N_p}{R_{sh}} \end{aligned} \quad (2)$$

where N_s and N_p are the number of solar cells in series and parallel, respectively.

1.3 Problem formulation

The task of extracting parameters for a solar PV model is typically reworked into a numerical optimization problem by minimizing the distance between the measured and simulated data [47, 48]. The error function employed is frequently expressed as the square root mean squared error (RMSE), as follows:

$$\mathrm{RMSE}(X) = \sqrt{\frac{1}{N}\sum_{i=1}^{N} f(U_{PV}, I_{PV}, X)^2} \quad (3)$$

where N denotes the number of measured I–V data.

In this study, Equation (3) is expressed as follows:

$$\begin{aligned} f(U_{PV}, I_{PV}, X) &= I_{ph} - I_{o1}\left\{\exp\left[\frac{q(U_{PV}+I_{PV}R_s)}{n_1kT}\right]-1\right\} \\ &-I_{o2}\left\{\exp\left[\frac{q(U_{PV}+I_{PV}R_s)}{n_2kT}\right]-1\right\} - \frac{U_{PV}+I_{PV}R_s}{R_{sh}} - I_{PV} \end{aligned} \quad (4)$$

$$X = \{R_s, R_{sh}, I_{ph}, I_{o1}, I_{o2}, n_1, n_2\} \quad (5)$$

On the other hand, in order to display the absolute error of the measured current and simulated current under each voltage, Equation (6) is used to express the difference between the real current value and the measured current value:

$$\text{Current Absolute Error} = |f(U_{PV}, I_{PV}, X)| \quad (6)$$

2 Parameter extraction of PV models

This study specifically selected two novel algorithms that have been validated and applied in engineering applications over the past 2 years for the purpose of extracting the seven parameters of solar cells. These two algorithms were then comprehensively compared with 15 other algorithms that have previously been employed in the field of solar cell parameter identification.

In addition to the algorithms mentioned above, the full names and abbreviations of other algorithms are as follows [20]: sparrow search algorithm (SSA), simulated annealing (SA), grey wolf optimizer (GWO), moth-flame optimization (MFO), multi-verse optimizer (MVO), salp swarm algorithm (SS), artificial vulture optimization algorithm (AVOA), gorilla troop optimizer (GTO), flow direction algorithm (FDA), pelican optimization algorithm (POA), chameleon swarm algorithm (CSA) and northern goshawk optimization (NGO).

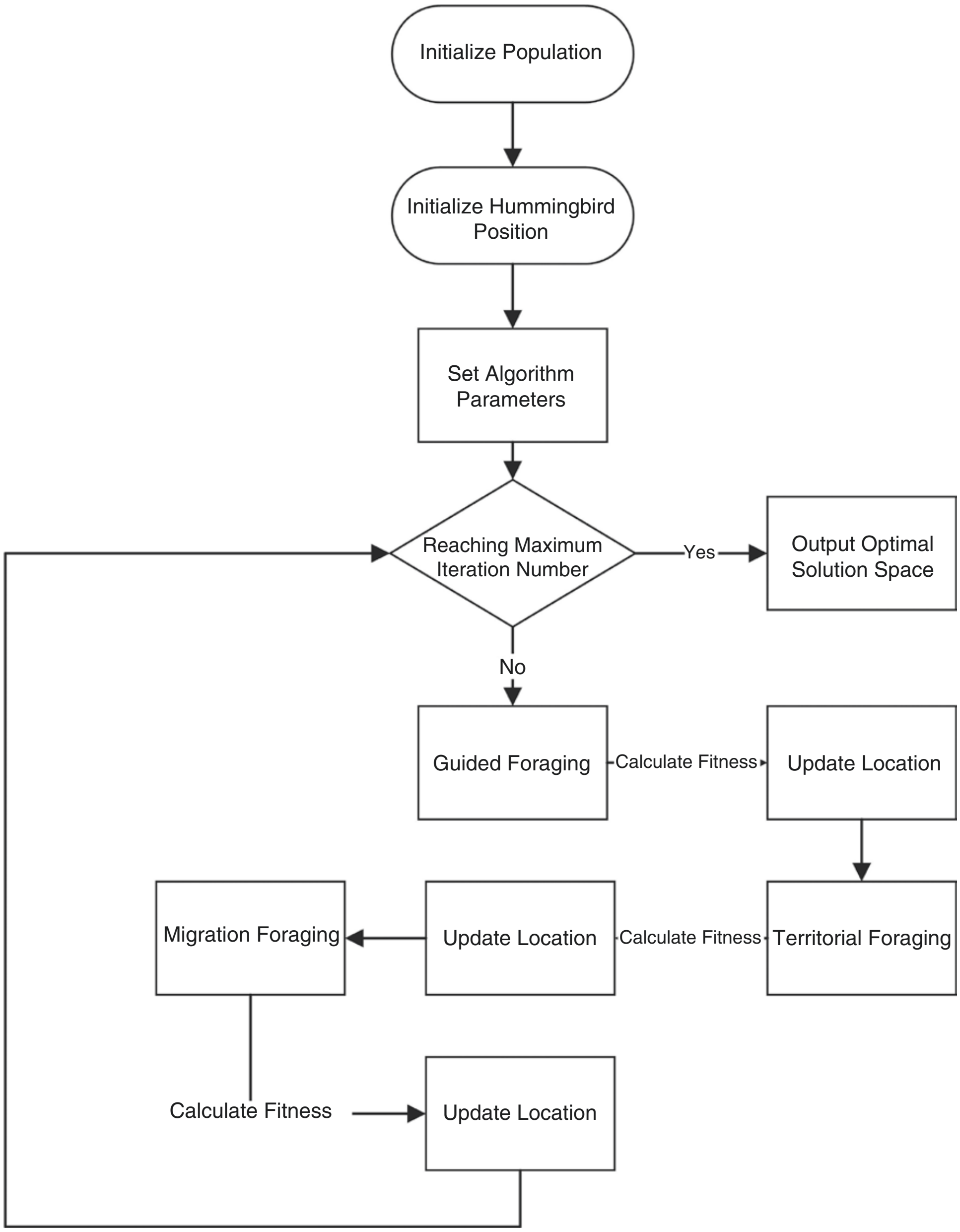

Fig. 3: The algorithm flowchart of AHA

Table 1: The parameters for the PV model

Type	Number of series	Number of parallels	Area (m^2)	I_{sc} (A)	V_{oc} (V)	I_m (A)	V_m (V)	P_m (W)
xSi12922	36	1	0.3429	4.9996	21.8684	4.5932	17.4484	80.1431

2.1 AHA

AHA is an optimization technique inspired by the foraging and flight of hummingbirds, as presented in [40].The three main models of this algorithm are presented as follows:

2.1.1 *Guided foraging*

In this foraging model, three flight behaviours are used in foraging (omnidirectional, diagonal and axial flight). Fig. 2 presents these three flight behaviours in 3D space. The equation simulating this guided foraging and a candidate food source can be obtained as follows:

$$v_i(t+1) = x_{i,ta}(t) + h.b.(x_i(t) - X_{i,ta}(t))h \sim N(0,1) \tag{7}$$

where $x_{i,ta}(t)$ represents the position of the target food source, h denotes the guided factor and follows the normal distribution of N (0,1) and $x_i(t)$ is the position of the i-th food source at time t.

The position update of the i-th food source is as follows:

$$x_i(t) = \begin{cases} x_i(t) & f(x_i(t)) \le f(v_i(t+1)) \\ v_i(t+1) & f(x_i(t)) > f(v_i(t+1)) \end{cases} \tag{8}$$

where $f(x_i(t))$ and $f(v_i(t+1))$ are the value of function fitness for $x_i(t)$ and $v_i(t+1)$, respectively.

Table 2: The search range of the parameters

Parameters	Value range
R_s (Ω)	[0, 5]
R_{sh} (Ω)	[0, 800]
I_{ph} (A)	[0, 6]
I_{o1} (A)	[0, 0.01]
I_{o2} (A)	[0, 0.01]
n_1	[0.8, 1.2]
n_2	[1.8, 2.2]

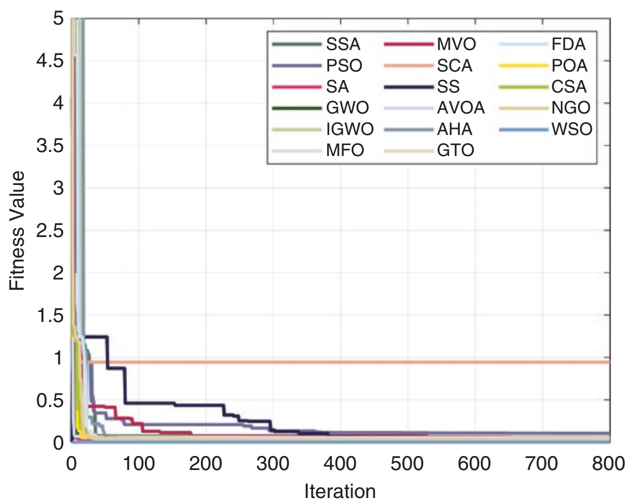

Fig. 4: The iteration process of 17 algorithms

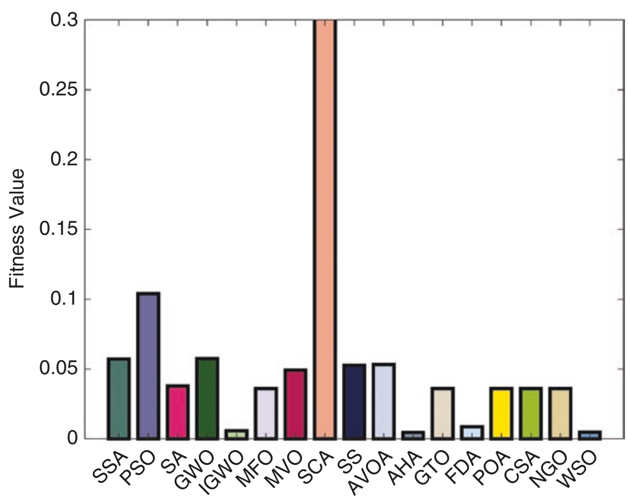

Fig. 5: The best values of the fitness function of 17 algorithms

2.1.2 *Territorial foraging*

The following equation represents the local search of hummingbirds in the territorial foraging strategy:

$$v_i(t+1) = x_i(t) + g.b.(x_i(t)) \quad g \sim N(0,1) \tag{9}$$

where g denotes the territorial factor and follows the normal distribution of N (0,1) and b denotes the D-dimensional solution space.

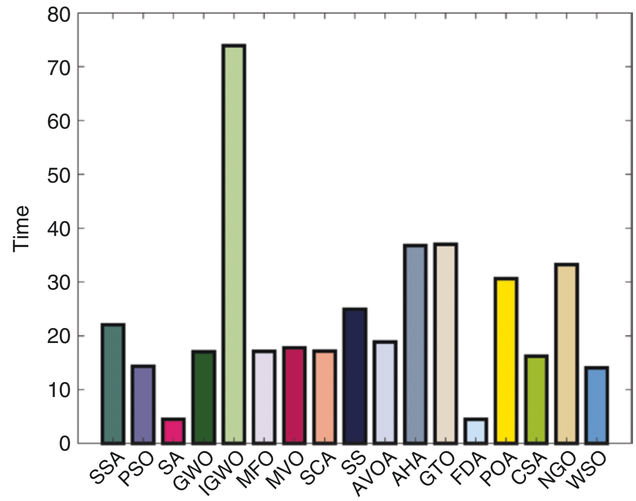

Fig. 6: The running time of 17 algorithms

2.1.3 *Migration foraging*

The mathematical equation for the migration foraging of a hummingbird is presented as follows:

$$x_{wor}(t+1) = lb + r.(ub - lb) \tag{10}$$

where x_{wor} represents the source of food with the worst population rate of nectar refilling, r is a random factor, and ub and lb are the upper and lower limit ranges, respectively.

The specific algorithm flowchart is shown in Fig. 3.

2.2 PV models

In this study, we applied data from the public data repository of the *I–V* curve established by the National Renewable Energy Laboratory (NREL) [49] for parameter estimation and result validation. NREL has measured numerous experimental data under different illumination and temperature conditions, including ~200 (*I–V*) data points collected every 5 or 15 minutes for various PV cells that cover 1 year.

The study used a large number of experimental *I–V* curves of PV cells made of multicrystalline silicon (mSi) and monocrystalline silicon (xSi) from Eugene for validation. Specifically, we selected 188 pairs of *I–V* data of monocrystalline silicon (xSi12922) under reference conditions with irradiance of 1012.7 W/m^2 and temperature of 24.9°C as the benchmark data; the module parameters are provided in Table 1. The data underlying this article are available in the article and in the online Supplementary Data.

2.3 Parameter extraction

The appropriate range of the parameter search plays a crucial role in determining the convergence interval and convergence rate of optimization algorithms, as well as ensuring the rationality of the parameters. Moreover, in order to prevent the extracted parameters from losing their physical meaning and becoming mere numerical values, it is necessary to fully understand the physical significance represented by each parameter and determine the suitable search range accordingly.

Due to the fact that the materials used to produce PV cells are not ideal conductors and possess a certain degree of resistance, it is necessary to incorporate a series resistance R_s [50, 51]. Additionally, cracks that are unavoidably generated in the manufacturing process may cause leakage within these gaps,

Table 3: The best extraction parameters and RMSE values for 17 algorithms

Algorithm	R_s (Ω)	R_{sh} (Ω)	I_{ph} (A)	I_{o1} (μA)	I_{o2} (μA)	n_1	n_2	RMSE (A)
SCA	0	0.267311	5.5	0	0	0.8	2.2	9.43E–01
PSO	–0.021347	381.072138	4.971673	3.53E+05	–9.84E+05	6.916198	12.803541	1.04E–01
GWO	5.65E–05	90.379642	5.004939	0	59.839329	0.864872	2.079667	5.74E–02
SSA	0	800	5.00018	0	57.055914	0.8	2.07054	5.72E–02
AVOA	0.000741	759.093363	5.004278	0	46.786369	1.017758	2.036336	5.324E–2
SS	0.000849	521.12508	5.004339	0	44.541544	0.80482	2.027975	5.27E–02
MVO	0.001306	750.96043	5.002829	0	33.351716	1.197479	1.978969	4.93E–02
SA	0.002727	800	4.994532	2.83E–05	12.093643	1.128449	1.825721	3.79E–02
MFO	0.002914	799.999999	4.993449	0	10.109841	0.8	1.8	3.61E–02
GTO	0.002914	800	4.993449	1.27E–25	10.109841	0.830664	1.8	3.61E–02
POA	0.002914	800	4.993457	0	10.109918	1.2	1.8	3.60E–02
CSA	0.002914	800	4.993449	1.08E–21	10.109841	0.810575	1.8	3.60E–02
NGO	0.002913	799.999999	4.993449	0	10.109841	0.895412	1.8	3.60E–02
FDA	0.006972	789.153975	4.976341	4.24E–03	3.231627	1.152771	1.8	8.70E–03
IGWO	0.007086	22.259203	4.985826	9.96E–03	4.034159	1.193525	1.896538	5.90E–03
WSO	**0.007179**	**13.116042**	**4.994842**	**7.33E–03**	**5.425701**	**1.174306**	**1.955255**	**4.70E–03**
AHA	**0.007187**	**12.905787**	**4.994944**	**4.41E–03**	**3.163286**	**1.149679**	**1.831975**	**4.62E–03**

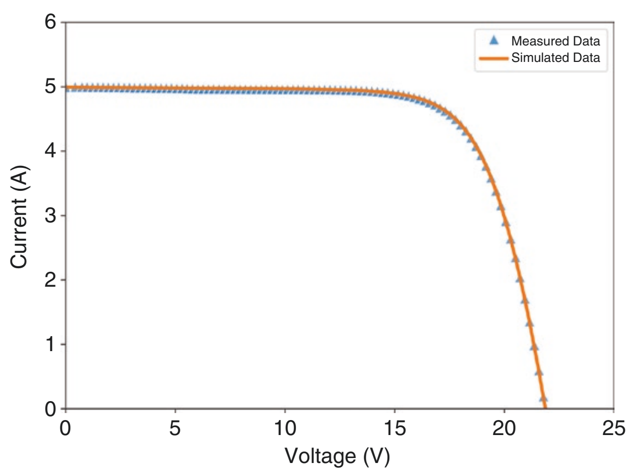

Fig. 7: Comparison of simulated data (AHA) and measured data

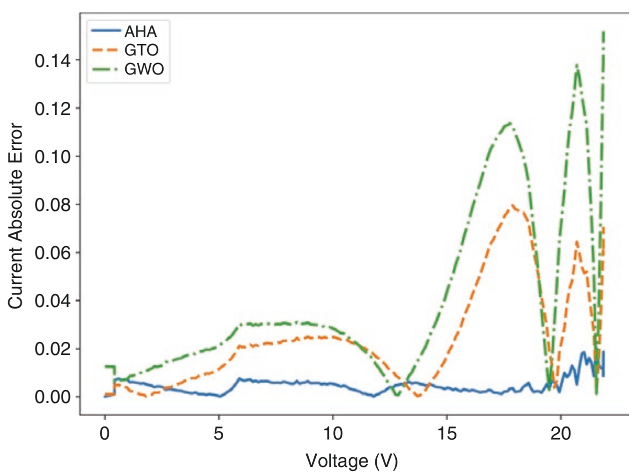

Fig. 8: The current absolute error of three algorithms

resulting in short circuits in the circuit. Hence, a shunt resistance R_{sh} needs to be added to prevent such short circuits [9,52,53]. R_s typically has a value of several ohms at most, while R_{sh} has a comparably larger value of hundreds of ohms [54–56]. The short-circuit current of the PV cell is determined by the photo current I_{ph}, which generally has a numerical value close to that of the short-circuit current [57–59]. The sizes of two reverse saturation currents I_{o1} and I_{o2} depend on the internal parameters of the diode and their values are relatively small [30,60,61], roughly in the order of 10^{-6} A.

Regarding the specific values of the ideality factors n_1 and n_2, it is challenging to measure them with equipment and express them in formulas. According to [62], it was assumed that the ideality factor of Diode 1 is equal to 1 and that of Diode 2 is >1.2, while [63] assumed that the ideality factor of Diode 1 is equal to that of Diode 2. However, these assumptions are not always correct. The ideality factor indicates how similar the characteristics of a diode are to an ideal diode. The value of the ideality factor generally ranges from 1 to 2, and improper selection of these values can significantly affect the accuracy of the model [41]. In this study, n_1 and n_2 were set at ~1 and ~2, respectively. Table 2 shows the search range of the parameters.

This study used the RMSE as the fitness function for parameter extraction. Sixteen other algorithms were selected for comparison and Fig. 4 shows the change in fitness function values of each algorithm during the iteration process. All heuristic algorithms continuously reduced their values of the fitness function during the iteration process and finally stabilized. Fig. 5 displays the best fitness function values of all heuristic algorithms during 800 iterations, while Fig. 6 shows the running time of all heuristic algorithms. The computer system used in this study was Windows 10, with an Intel(R) Core(TM) i7-7700HQ CPU @ 2.80GHz 2.80 GHz processor. All codes were programmed using MATLAB® 2022a. The initial population for all algorithms was set at 400, with a maximum iteration of 800.

The best extraction parameters and corresponding RMSE values for various algorithms in the DD model, sorted into descending order of their RMSE values, are presented in Table 3.

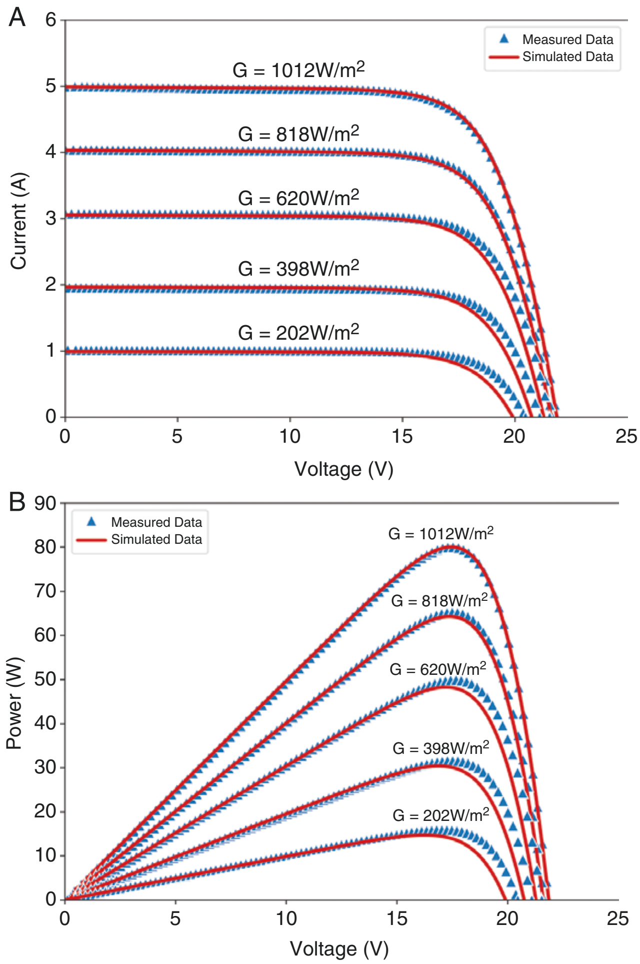

Fig. 9: Measured and simulated data under different irradiances. (a) *I–V* characteristic curve; (b) *P–V* characteristic curve.

The simulated data obtained by applying the seven parameters calculated by using AHA to the current output equation of the PV module is compared with the measured data, as shown in Fig. 7.

When selecting the three algorithms with representative RMSE from the above algorithm, the simulated output current values are calculated using their extracted parameters and then compared with the actual measured values under reference conditions with irradiance of 1012.7 W/m² and temperature of 24.9°C. The absolute error of the output current is shown in Fig. 8.

As shown in Fig. 8, it can be observed that the AHA algorithm has smaller output current errors within the input voltage range and better stability compared with the other algorithms. It should be noted that all algorithms have a sharp increase in the computed errors near the open-circuit voltage. This is due to the difficulty in accurately measuring current values near the open-circuit voltage using measurement equipment. Fortunately, this does not affect the overall output characteristics of the PV cell.

3 Results and discussion

3.1 Application of extraction parameters

PV modules operate under different weather conditions and their parameters are therefore influenced by temperature and irradiance. However, all parameters are given under standard test conditions. As a result, extrapolating all these parameters to different operating conditions is crucial. The dependence of the PV model parameters on temperature and irradiance can generally be incorporated into the mathematical model using a suitable set of translation formulas [64]. Using this approach, a *I–V* relationship was achieved that took into account the irradiance and temperature conditions. Supervised principles [65] were used to consider the dependence on temperature and irradiance levels in this relationship mathematically. Combining the parameter modification methods proposed in [64, 66], this study adopted the following modification methods.

The photo current:

$$I_{ph} = \frac{G}{Gref}\left[Iph, ref + \alpha Isc\left(T - Tref\right)\right] \tag{11}$$

The reverse saturation currents:

$$I_{o1} = I_{o1,ref}\left(\frac{T}{T_{ref}}\right)^{3} \exp\left[\frac{1}{n_1 K}\left(\frac{E_{G,ref}}{T_{ref}} - \frac{E_G}{T}\right)\right] \tag{12}$$

$$I_{o2} = I_{o2,ref}\left(\frac{T}{T_{ref}}\right)^{3} \exp\left[\frac{1}{n_2 K}\left(\frac{E_{G,ref}}{T_{ref}} - \frac{E_G}{T}\right)\right] \tag{13}$$

The resistances:

$$Rs = Rs, ref\left(\frac{T}{Tref}\right)^{3}\left(1 - 0.217\ln\left(\frac{G}{G_{ref}}\right)\right) \tag{14}$$

$$Rsh = \frac{Gref}{G} Rsh, ref \tag{15}$$

The subscript '*ref*' denotes the values of different parameters under the reference condition. For the bandgap energy of the material, for silicon solar cells, its value at T_{STC} = 25°C is set at 1.121 eV. The value is provided as a function of the cell temperature.

The band gap energy:

$$E_G = 1.16 - \frac{7.02 \times 10^{-4} T^2}{1108 + T}[eV] \tag{16}$$

The ideal factors:

$$n1 = n1, ref \tag{17}$$

$$n2 = n2, ref \tag{18}$$

Using the above modifications, the *I–V* and *P–U* curves are simulated under different levels of irradiance and compared with real measured data as shown in Fig. 9.

It is observed that the simulated data have significant deviations at low irradiance levels, mainly due to the overall downward shift of the simulated data in the non-linear section between the maximum power point and the open-circuit voltage point compared with the measured data. Therefore, it is necessary to analyse the effect of each parameter on the curves.

3.2 Sensitivity analysis of seven parameters

The physical meanings of the seven parameters have been briefly explained earlier. Among them, I_{ph} appears separately in the DD output equation and is not coupled with other parameters, making it easier to analyse. From the diode circuit diagram, it can be seen that I_{ph} is the source of the PV cell output current and its magnitude determines the maximum value of the output current, namely the short-circuit current. It can be seen from the curve that the corrected value of I_{ph} is reasonable, as there is no significant deviation near the short-circuit current.

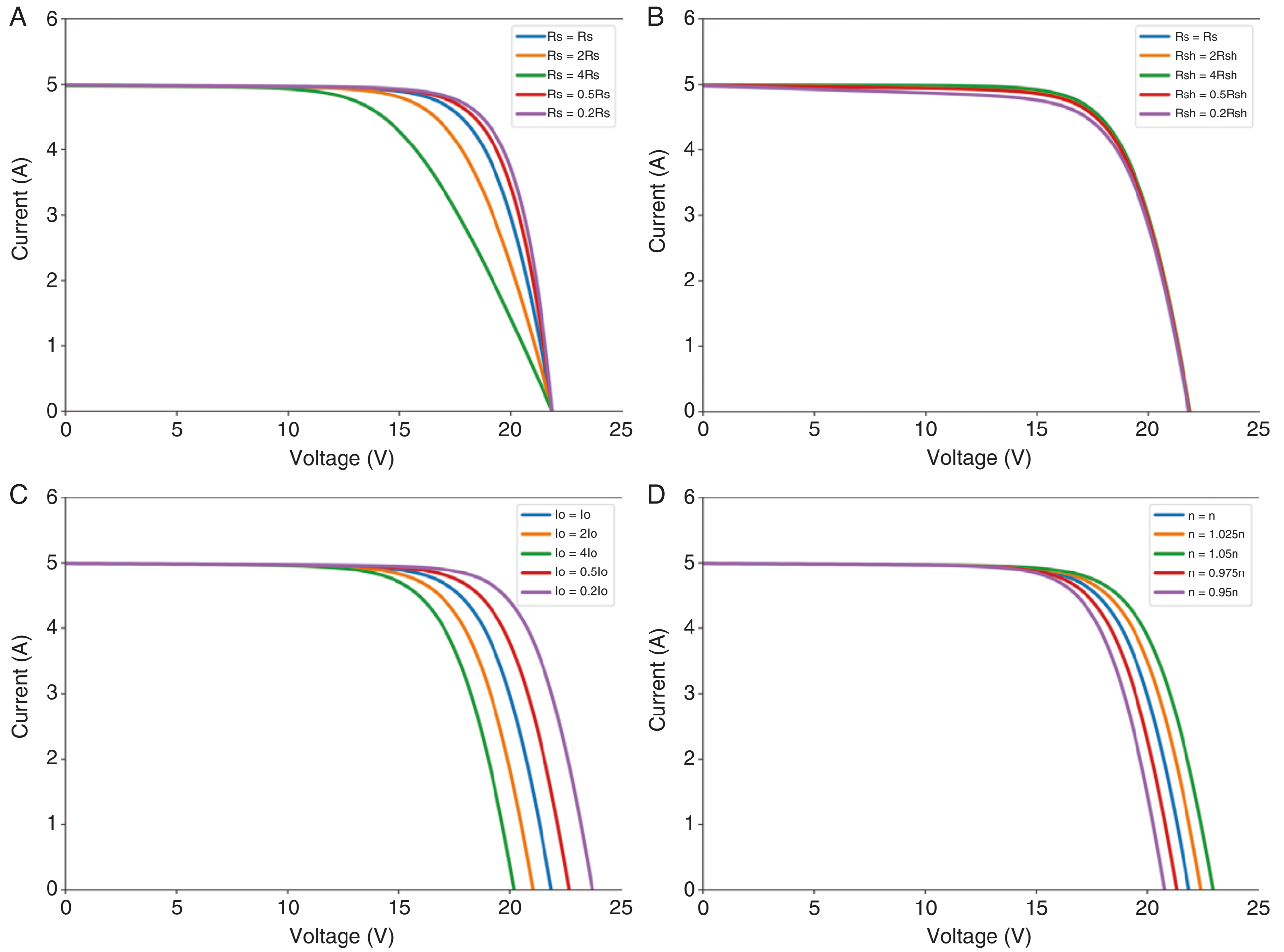

Fig. 10: Impact of parameter sensitivity. (a) The impact of R_s sensitivity; (b) the impact of R_{sh} sensitivity; (c) the impact of I_o sensitivity; (d) the impact of n sensitivity.

The other six parameters have complex relationships, making immediate analysis difficult. In this study, the impact of the six parameters on the curves was identified to judge the possible problems with parameter corrections.

The simulation curve obtained by appropriately scaling the other six parameters obtained under the reference conditions is compared with the original curve, as shown in Fig. 10.

It can be seen that the impact of the series resistance R_s and the shunt resistance R_{sh} on the curve is reflected in the deviation of the maximum power point inward or outward, and the influence of R_{sh} is negligible. However, the deviations of the curves in Figs. 10a and b are not consistent with those shown in Fig. 9, indicating that there is no issue with the parameter correction for R_s and R_{sh}.

Regarding the reverse saturation currents I_{o1} and I_{o2}, as well as their corresponding ideality factors n_1 and n_2, since they represent the same physical characteristics, their changes should be synchronous. Therefore, in the following study, I_o is used to denote the synchronous variations of I_{o1} and I_{o2}, and n is used to denote the synchronous variations of n_1 and n_2.

As shown in Figs 10c and d, the influence of I_o and n on the curve is similar, both of which can cause the curve to shift downward as a whole in the non-linear range. It can be surmised that errors in the correction of I_o and n in the seven-parameter adjustment under different radiation intensities may lead to deviations in the simulated data.

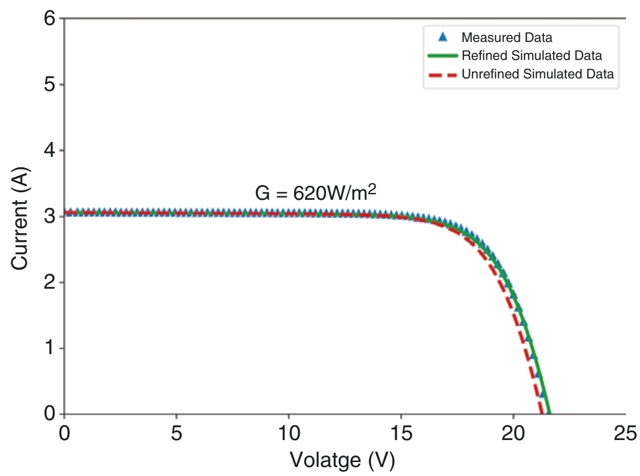

Fig. 11: Refined simulated data and unrefined simulated data for $G = 620\ W/m^2$

Furthermore, it should be noted that even a small scaling of the value of n can cause significant deviations in the curve. The I_o correction expression only contains the correction of T and the change in the I_o value due to the variation in radiation intensity is not affected. At the same time, as shown in Equation (1), the change in the n value will also cause a change in the factor multiplied by I_o. Therefore, the

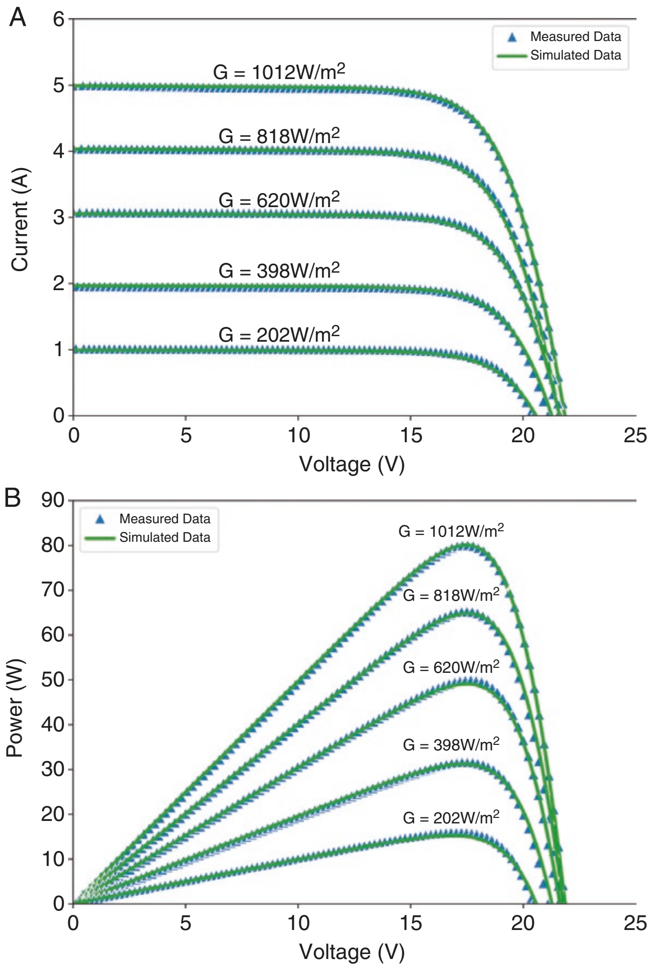

Fig. 12: Refined simulated data and measured data under different irradiances. (a) *I–V* characteristic curve; (b) *P–V* characteristic curve.

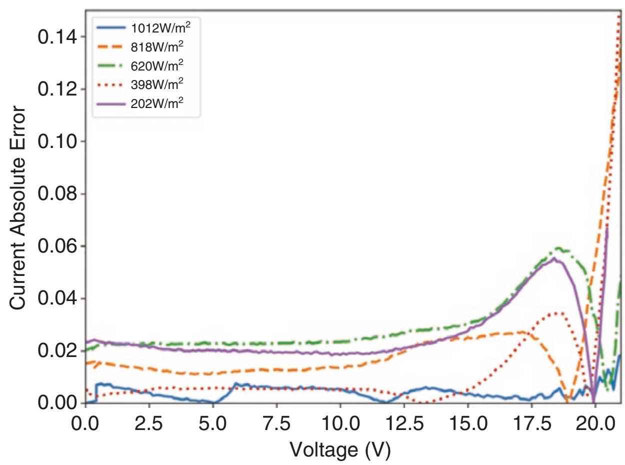

Fig. 13: The current absolute error under different irradiances

influence of n is reflected not only in the shift of the curve, but also in the change in the factor multiplied by I_o. That means that the change in the n value will be converted into a change in the I_o value. Therefore, the influence of I_o and n on the curve is similar.

3.3 Modification of the ideal factors

Due to the difficulty in determining the relationship between the ideality factor and the light intensity or temperature in most literature, n values are usually not corrected under actual conditions and are directly adopted based on their reference conditions.

However, Ghani *et al.* [67], Khan *et al.* [68], Cuce *et al.* [69] and Deshmukh *et al.* [70] suggest that the ideality factor decreases linearly with an increase in temperature, while Khan *et al.* [71] and Singh *et al.* [72] believe that it remains nearly constant. Chegaar *et al.* [73] and Khan *et al.* [74] found that the ideality factor increases with an increase in light intensity, while Khan *et al.* [75] suggest that it decreases with an increase in light intensity. Additionally, Lim *et al.* [76] proposed that the dependence of the ideality factor on the light intensity is not monotonic.

In summary, most scholars believe that the ideality factor is highly insensitive to environmental conditions and can even be

Table 4: The RMSE values for each irradiance

G (W/m²)	RMSE (A)
1012	0.0062
818	0.0495
620	0.0360
398	0.0338
202	0.0288

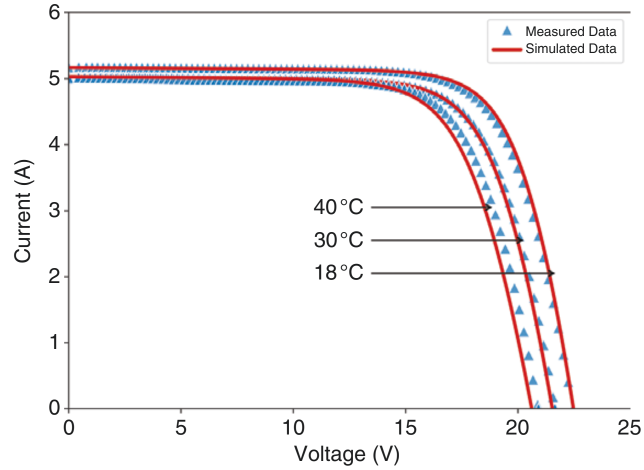

Fig. 14: The measured data and the simulated data at different temperatures

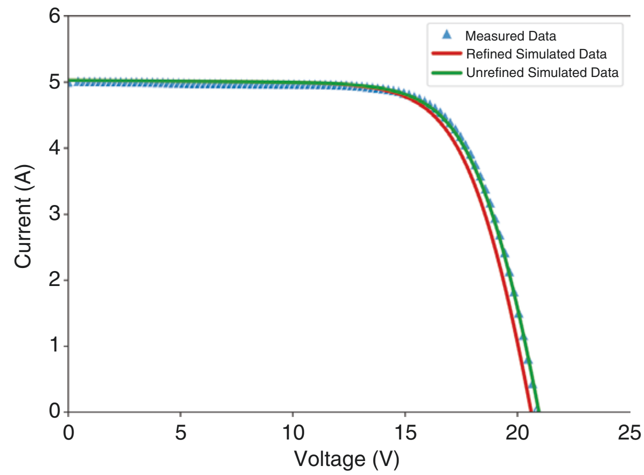

Fig. 15: Refined simulated data and unrefined simulated data for $T = 30°C$

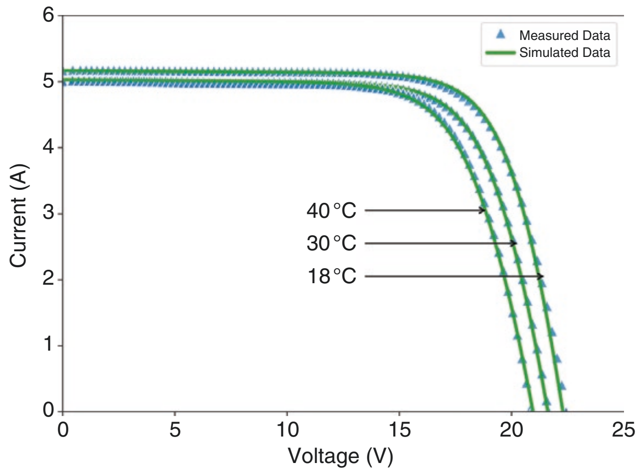

Fig. 16: Refined simulated data and measured data at different temperatures

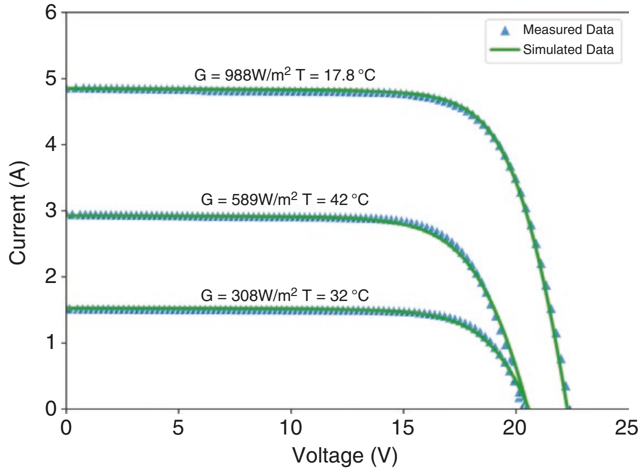

Fig. 18: Refined simulated data and measured data under comprehensive conditions

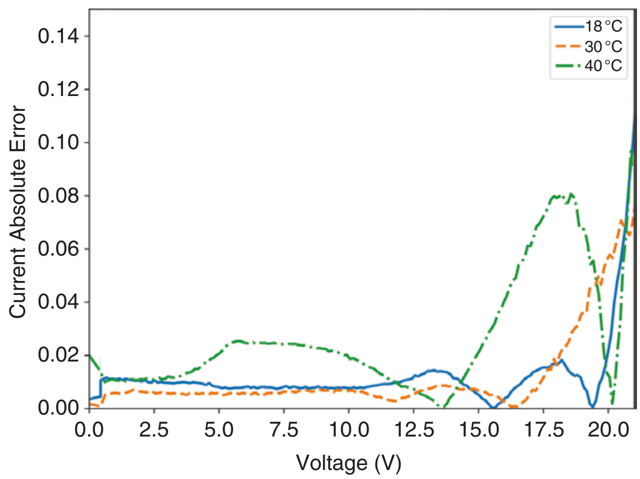

Fig. 17: The current absolute error under different temperatures

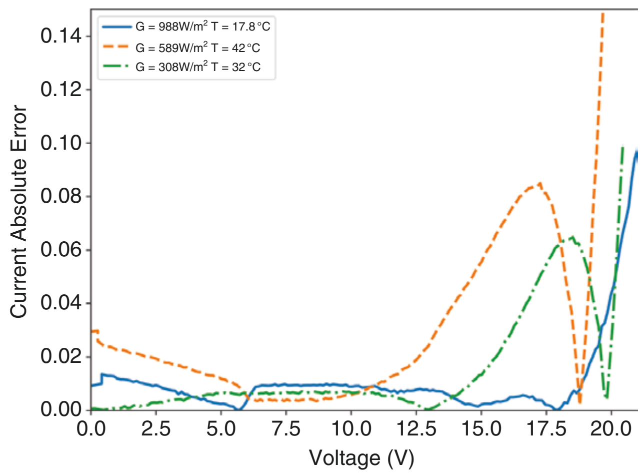

Fig. 19: The current absolute error under comprehensive conditions

Table 5: The RMSE values for each temperature

T (℃)	RMSE (A)
18	0.0282
30	0.0257
40	0.0364

Table 6: The RMSE values under various conditions

Condition	RMSE (A)
G = 988 W/m², T = 17.8℃	0.0697
G = 589 W/m², T = 42℃	0.0570
G = 308 W/m², T = 32℃	0.0289

ignored. However, from the graph, it can be observed that even slight variations in the ideality factor can have a significant impact on the output curve. Therefore, this study needs to make certain modifications to the ideality factor to match the output curve in different situations.

Since the magnitude of the variation in the ideality factor is minimal, this study uses a linear variation of the ideality factor with respect to irradiance for correction purposes.

3.3.1 *Modification under irradiance*

To begin with, the curve corresponding to $G = 620$ W/m², $T = 24.9$℃ was selected for the correction of the parameters. Following a thorough verification, it was established that the modification of the ideality factor as $n = (1 + 0.016)n_{ref}$ resulted in data that were more closely aligned with experimental observations compared with unrefined data. A comparison of the refined and unrefined data against experimental data, shown in Fig. 11, highlights a superior conformity of the corrected data to the experimental trends.

Therefore, Equation (19) was utilized to correct and validate the data at other irradiance levels ($G = 1012$, 818, 398 and 202 W/m²) under $T = 24.9$℃, as shown in Fig. 11:

$$n = n_{ref} \times \left[1 + \frac{0.016}{1012.7 - 620} \times (G_{ref} - G)\right] \tag{19}$$

Based on Fig. 12, it can be observed that, to a certain extent, the linear expression for the irradiance correction of ideal factors exhibits a degree of universality.

Fig. 13 illustrates the absolute error of the output current under different levels of irradiance. As mentioned earlier, it is difficult for the measuring instrument to accurately measure the current value near the open-circuit voltage. For example, negative values of current are frequently measured around the open-circuit voltage, leading to a significant increase in error values near the open-circuit voltage. Therefore, the simulated data error conforms to the actual characteristics.

The RMSE values for each irradiance are shown in Table 4.

3.3.2 *Modification under temperature*

We will now employ the same methodology to verify the performance of simulated data at different temperatures. Due to the measurement data, the control data with identical irradiance but different temperatures cannot be obtained. Therefore, three groups of data, namely $T = 18°C$, $G = 1052\ W/m^2$, $T = 30°C$, $G = 1018\ W/m^2$ and $T = 40°C$, $G = 1012\ W/m^2$, are selected in this section for the study of temperature correction. The simulated data and the measured data under these three conditions are shown in Fig. 14.

It can be observed from Fig. 13 that similar issues to those seen under different irradiance levels also arise in the simulated data under different temperatures. Considering that the ideal factor n is sensitive to temperature to some extent, we adopt the same methodology to correct the ideal factor for temperature. First, we corrected the curve for $T = 30$ °C and, through several verifications, found that when $n = (1 + 0.005)n_{ref}$, the corrected data were more consistent with the experimental data compared with the uncorrected data, as shown in Fig. 15.

Therefore, Equation (20) was used to correct and validate the data at other temperature levels, resulting in the results shown in Fig. 16:

$$n = n_{ref} \times \left[1 + \frac{0.005}{30 - 25} \times (T - T_{ref})\right] \tag{20}$$

Based on Fig. 16, it can be observed that, to a certain extent, the linear expression for temperature correction of ideal factors also exhibits a degree of universality. Fig. 17 illustrates the absolute error of output current under different temperature levels.

The RMSE values for each temperature are shown in Table 5.

3.3.3 *Modification under comprehensive conditions*

When the corrections for temperature and irradiance are combined, the linear superposition of their influences on the ideal factor is obtained. Based on this, the present study proposes Equation (21) for the correction of the ideal factor under different temperature and irradiance conditions:

$$n = n_{ref} \times \left[1 + \left(\frac{0.016}{1012.7 - 620} \times (G_{ref} - G) + \frac{0.005}{30 - 25} \times (T - T_{ref})\right)\right] \tag{21}$$

The present study also randomly selected data under different temperature and irradiance conditions to further validate the corrected parameters, as shown in Fig. 18. Fig. 19 illustrates the absolute error of the output current under those conditions.

The RMSE values under each condition are shown in Table 6.

Although the absolute error of the output current under composite conditions seems to be larger than that under single conditions, it is completely acceptable considering the error of the measuring instrument under real conditions and the difference between the actual and the physical models, and the output current of the module is often one order of magnitude higher than the absolute error.

4 Conclusion

This paper briefly introduces the existing parameter extraction methods and uses the latest metaheuristic algorithm to solve the problem of the nonlinearity, multivariable and multimode of PV cell dual diodes, thus extracting the seven parameters of PV cells. The new algorithm is compared with classic parameter extraction algorithms to verify its applicability and accuracy in the field of parameter extraction. Considering practicality in engineering, this study combines the advantages of metaheuristic algorithms in parameter extraction and the advantages of analytical methods in reference condition-based parameter correction to propose a method of performing parameter correction after parameter extraction using metaheuristic algorithms to meet engineering applications. In particular, on the deviation observed in the simulated data, this study has proposed targeted corrections for the ideal factor of the diode under different conditions to further improve the accuracy of the model.

Supplementary data

Supplementary data is available at *Clean Energy* online.

Acknowledgements

I would like to thank my supervisor, Dr Jun Wang, for his guidance through each stage of the process, whose expertise was invaluable in formulating the research questions and methodology. His insightful feedback pushed me to sharpen my thinking and brought my work to a higher level.

Funding

This research did not receive any specific grant from funding agencies in the public, commercial or not-for-profit sectors.

Conflict of interest statement

None declared.

Data Availability

The raw data underlying this article are available in [EMN-DURMAT (EMN-DuraMAT)], at https://dx.doi.org/10.21948/1811521. The applied data underlying this article are available in the online Supplementary Data.

References

[1] Chin VJ, Salam Z, Ishaque K. Cell modelling and model parameters estimation techniques for photovoltaic simulator application: a review. *Appl Energy*, 2015, 154:500–519.

[2] Tina G. A coupled electrical and thermal model for photovoltaic modules. *J Sol Energy Eng*, 2010, 132:024501.

[3] Hejri M, Mokhtari H, Azizian MR, *et al*. An analytical-numerical approach for parameter determination of a five-parameter single-diode model of photovoltaic cells and modules. *Int J Sustainable Energy*, 2016, 35:396–410.

[4] Accarino J, Petrone G, Ramos-Paja CA, *et al*. Symbolic algebra for the calculation of the series and parallel resistances in PV module model. In: *2013 International Conference on Clean Electrical Power (ICCEP)*, Alghero, Italy, 11–13 June 2013, 62–66.

[5] Villalva MG, Gazoli JR, Filho ER. Comprehensive approach to modeling and simulation of photovoltaic arrays. *IEEE Trans Power Electron*, 2009, 24:1198–1208.

[6] Louzazni M, Khouya A, Crăciunescu A, *et al*. Modelling and parameters extraction of flexible amorphous silicon solar cell a-Si:H. *Appl Sol Energy*, 2020, 56:1–12.

[7] Chenni R, Makhlouf M, Kerbache T, *et al*. A detailed modeling method for photovoltaic cells. *Energy*, 2007, 32:1724–1730.

[8] Polman A, Van Sark WGJHM, Sinke W, *et al*. A new method for the evaluation of solar cell parameters. *Sol Cells*, 1986, 17:241–251.

[9] Adamo F, Attivissimo F, Di Nisio A, *et al*. Characterization and testing of a tool for photovoltaic panel modeling. *IEEE Trans Instrum Meas*, 2011, 60:1613–1622.

[10] Gow JA, Manning CD. Development of a photovoltaic array model for use in power-electronics simulation studies. *IEE Proc Electr Power Appl*, 1999, 146:193.

[11] Yordanov GH, Midtgård O-M, Sætre TO. Two-diode model revisited: parameters extraction from semi-log plots of I-V data. In: *25th European Photovoltaic Solar Energy Conference and Exhibition/5th World Conference on Photovoltaic Energy Conversion*, Valencia, Spain, 6–10 September 2010, 4156–4163.

[12] Dolan JA, Lee R, Yeh Y-H, *et al*. Neural network estimation of photovoltaic I-V curves under partially shaded conditions. In: *2011 International Joint Conference on Neural Networks*, San Jose, CA, USA, 31 July–5 August 2011, 1358–1365.

[13] Enebish N, Agchbayar D, Dorjkhand S, *et al*. Numerical analysis of solar cell current-voltage characteristics. *Sol Energy Mater Sol Cells*, 1993, 29:201–208.

[14] Tamrakar R, Gupta A. A review extraction of solar cell modelling parameters. *International Journal of Innovative Research in Electrical, Electronics. Instrum Control Eng*, 2015, 3:55–60.

[15] Chen C, Kang Y, Huo Z, *et al*. Highly crystalline multimetallic nanoframes with three-dimensional electrocatalytic surfaces. *Science*, 2014, 343:1339–1343.

[16] Hovinen A. Fitting of the solar cell IV-curve to the two diode model. *Phys Scr*, 1994, T54:175–176.

[17] Chen X, Yu K, Du W, *et al*. Parameters identification of solar cell models using generalized oppositional teaching learning based optimization. *Energy*, 2016, 99:170–180.

[18] Kumar M, Kumar A. An efficient parameters extraction technique of photovoltaic models for performance assessment. *Sol Energy*, 2017, 158:192–206.

[19] Bryant FJ, Glew RW. Analysis of the current-voltage characteristics of cadmium sulphide solar cells under varying light intensities. *Energy Convers*, 1975, 14:129–133.

[20] Li S, Gong W, Gu Q. A comprehensive survey on meta-heuristic algorithms for parameter extraction of photovoltaic models. *Renew Sustain Energy Rev*, 2021, 141:110828.

[21] Peng L, Sun Y, Meng Z, *et al*. A new method for determining the characteristics of solar cells. *J Power Sources*, 2013, 227:131–136.

[22] Chen Y, Wang X, Li D, *et al*. Parameters extraction from commercial solar cells I–V characteristics and shunt analysis. *Appl Energy*, 2011, 88:2239–2244.

[23] Gao X, Cui Y, Hu J, *et al*. Lambert W-function based exact representation for double diode model of solar cells: comparison on fitness and parameter extraction. *Energy Convers Manage*, 2016, 127:443–460.

[24] Chan DSH, Phang JCH. Analytical methods for the extraction of solar-cell single- and double-diode model parameters from I-V characteristics. *IEEE Trans Electron Devices*, 1987, 34:286–293.

[25] Jordehi AR. Parameter estimation of solar photovoltaic (PV) cells: a review. *Renew Sustain Energy Rev*, 2016, 61:354–371.

[26] Pillai DS, Rajasekar N. Metaheuristic algorithms for PV parameter identification: a comprehensive review with an application to threshold setting for fault detection in PV systems. *Renew Sustain Energy Rev*, 2018, 82:3503–3525.

[27] Wolf P, Benda V. Identification of PV solar cells and modules parameters by combining statistical and analytical methods. *Sol Energy*, 2013, 93:151–157.

[28] Fathy A. Recent meta-heuristic grasshopper optimization algorithm for optimal reconfiguration of partially shaded PV array. *Sol Energy*, 2018, 171:638–651.

[29] Balasubramanian K, Jacob B, Priya K, *et al*. Critical evaluation of genetic algorithm based fuel cell parameter extraction. *Energy Procedia*, 2015, 75:1975–1982.

[30] Ismail MS, Moghavvemi M, Mahlia TMI. Characterization of PV panel and global optimization of its model parameters using genetic algorithm. *Energy Convers Manage*, 2013, 73:10–25.

[31] Nunes HGG, Pombo JAN, Mariano SJPS, *et al*. A new high performance method for determining the parameters of PV cells and modules based on guaranteed convergence particle swarm optimization. *Appl Energy*, 2018, 211:774–791.

[32] Rezaee Jordehi A. Enhanced leader particle swarm optimisation (ELPSO): an efficient algorithm for parameter estimation of photovoltaic (PV) cells and modules. *Sol Energy*, 2018, 159:78–87.

[33] Yousri D, Allam D, Eteiba MB, *et al*. Static and dynamic photovoltaic models' parameters identification using chaotic heterogeneous comprehensive learning particle swarm optimizer variants. *Energy Convers Manage*, 2019, 182:546–563.

[34] Ishaque K, Salam Z, Mekhilef S, *et al*. Parameter extraction of solar photovoltaic modules using penalty-based differential evolution. *Appl Energy*, 2012, 99:297–308.

[35] Abd Elaziz M, Oliva D. Parameter estimation of solar cells diode models by an improved opposition-based whale optimization algorithm. *Energy Convers Manage*, 2018, 171:1843–1859.

[36] Li S, Gong W, Yan X, *et al*. Parameter estimation of photovoltaic models with memetic adaptive differential evolution. *Sol Energy*, 2019, 190:465–474.

[37] Chen H, Jiao S, Heidari AA, *et al*. An opposition-based sine cosine approach with local search for parameter estimation of photovoltaic models. *Energy Convers Manage*, 2019, 195:927–942.

[38] Nadimi-Shahraki MH, Taghian S, Mirjalili S. An improved grey wolf optimizer for solving engineering problems. *Expert Syst Appl*, 2021, 166:113917.

[39] Braik M, Hammouri A, Atwan J, *et al*. White shark optimizer: a novel bio-inspired meta-heuristic algorithm for global optimization problems. *Knowledge-Based Systems*, 2022, 243:108457.

[40] Zhao W, Wang L, Mirjalili S. Artificial hummingbird algorithm: a new bio-inspired optimizer with its engineering applications. *Comput Methods Appl Mech Eng*, 2022, 388:114194.

[41] Chennoufi K, Ferfra M, Mokhlis M. An accurate modelling of photovoltaic modules based on two-diode model. *Renew Energy*, 2021, 167:294–305.

[42] Ram JP, Babu TS, Dragicevic T, *et al*. A new hybrid bee pollinator flower pollination algorithm for solar PV parameter estimation. *Energy Convers Manage*, 2017, 135:463–476.

[43] Diabat A, Kannan D, Kaliyan M, *et al*. An optimization model for product returns using genetic algorithms and artificial immune system. *Resour Conserv Recycl*, 2013, 74:156–169.

[44] Zhang S, Luo Q, Zhou Y. Hybrid grey wolf optimizer using elite opposition-based learning strategy and simplex method. *Int J Comp Intel Appl*, 2017, 16:1750012.

[45] Chen X, Yu K. Hybridizing cuckoo search algorithm with biogeography-based optimization for estimating photovoltaic model parameters. *Sol Energy*, 2019, 180:192–206.

[46] Gong W, Cai Z. Parameter extraction of solar cell models using repaired adaptive differential evolution. *Sol Energy*, 2013, 94:209–220.
[47] Kler D, Sharma P, Banerjee A, *et al*. PV cell and module efficient parameters estimation using evaporation rate based water cycle algorithm. *Swarm Evol Comput*, 2017, 35:93–110.
[48] Long W, Cai S, Jiao J, *et al*. A new hybrid algorithm based on grey wolf optimizer and cuckoo search for parameter extraction of solar photovoltaic models. *Energy Convers Manage*, 2020, 203:112243.
[49] Marion B, Anderberg A, Deline C, *et al*. *Data for Validating Models for PV Module Performance*. EMN-DURMAT (EMN-DuraMAT), Golden, CO, USA: National Renewable Energy Laboratory (NREL), 2021.
[50] Schroder DK, Meier DL. Solar cell contact resistance: a review. *IEEE Trans Electron Devices*, 1984, 31:637–647.
[51] Barbato M, Meneghini M, Cester A, *et al*. Influence of shunt resistance on the performance of an illuminated string of solar cells: theory, simulation, and experimental analysis. *IEEE Trans Device Mater Reliab*, 2014, 14:942–950.
[52] Bharathraj S, Lee M, Adiga SP, *et al*. Detection, classification and quantification of short circuits in batteries using a short fatigue metric. *J Storage Mater*, 2023, 61:106729.
[53] Sera D, Teodorescu R, Rodriguez P. PV panel model based on datasheet values. In: *2007 IEEE International Symposium on Industrial Electronics*, Vigo, Spain, 4–7 June 2007, 2392–2396.
[54] Simon J, Andre J-J. *Molecular Semiconductors: Photoelectrical Properties and Solar Cells*. Berlin, Germany: Springer Science & Business Media, 2012.
[55] Mahmoud YA, Xiao W, Zeineldin HH. A parameterization approach for enhancing PV model accuracy. *IEEE Trans Ind Electron*, 2013, 60:5708–5716.
[56] Rajkanan K, Shewchun J. A better approach to the evaluation of the series resistance of solar cells. *Solid-State Electron*, 1979, 22:193–197.
[57] Masmoudi F, Ben Salem F, Derbel N. Single and double diode models for conventional mono-crystalline solar cell with extraction of internal parameters. In: *2016 13th International Multi-Conference on Systems, Signals & Devices (SSD)*, Leipzig, Germany, 21–24 March 2016, 720–728.
[58] Adak S, Cangi H, Yilmaz AS, *et al*. Development software program for extraction of photovoltaic cell equivalent circuit model parameters based on the Newton–Raphson method. *J Comput Electron*, 2023, 22:413–422.
[59] Motahhir S, El Ghzizal A, Sebti S, *et al*. Modeling of photovoltaic system with modified incremental conductance algorithm for fast changes of irradiance. *Int J Photoenergy*, 2018, 2018:3286479.
[60] Orioli A, Di Gangi A. A procedure to evaluate the seven parameters of the two-diode model for photovoltaic modules. *Renew Energy*, 2019, 139:582–599.
[61] Shaheen AM, El-Seheimy RA, Xiong G, *et al*. Parameter identification of solar photovoltaic cell and module models via supply demand optimizer. *Ain Shams Eng J*, 2022, 13:101705.
[62] Ishaque K, Salam Z, Taheri H. Simple, fast and accurate two-diode model for photovoltaic modules. *Sol Energy Mater Sol Cells*, 2011, 95:586–594.
[63] Lun S, Wang S, Yang G, *et al*. A new explicit double-diode modeling method based on Lambert W-function for photovoltaic arrays. *Sol Energy*, 2015, 116:69–82.
[64] Hejri M, Mokhtari H, Azizian MR, *et al*. On the parameter extraction of a five-parameter double-diode model of photovoltaic cells and modules. *IEEE J Photovoltaics*, 2014, 4:915–923.
[65] Boyd MT, Klein SA, Reindl DT, *et al*. Evaluation and validation of equivalent circuit photovoltaic solar cell performance models. *J Sol Energy Eng*, 2011, 133:021005. https://doi.org/10.1115/1.4003584.
[66] De Soto W, Klein SA, Beckman WA. Improvement and validation of a model for photovoltaic array performance. *Sol Energy*, 2006, 80:78–88.
[67] Ghani F, Rosengarten G, Duke M, *et al*. On the influence of temperature on crystalline silicon solar cell characterisation parameters. *Sol Energy*, 2015, 112:437–445.
[68] Khan F, Baek S-H, Kim JH. Wide range temperature dependence of analytical photovoltaic cell parameters for silicon solar cells under high illumination conditions. *Appl Energy*, 2016, 183:715–724.
[69] Cuce E, Cuce PM, Bali T. An experimental analysis of illumination intensity and temperature dependency of photovoltaic cell parameters. *Appl Energy*, 2013, 111:374–382.
[70] Deshmukh MP, Nagaraju J. Measurement of silicon and GaAs/Ge solar cell device parameters. *Sol Energy Mater Sol Cells*, 2005, 89:403–408.
[71] Khan F, Baek S-H, Park Y, *et al*. Extraction of diode parameters of silicon solar cells under high illumination conditions. *Energy Convers Manage*, 2013, 76:421–429.
[72] Singh P, Singh SN, Lal M, *et al*. Temperature dependence of I–V characteristics and performance parameters of silicon solar cell. *Sol Energy Mater Sol Cells*, 2008, 92:1611–1616.
[73] Chegaar M, Hamzaoui A, Namoda A, *et al*. Effect of illumination intensity on solar cells parameters. *Energy Procedia*, 2013, 36:722–729.
[74] Khan F, Baek S-H, Kim JH. Intensity dependency of photovoltaic cell parameters under high illumination conditions: an analysis. *Appl Energy*, 2014, 133:356–362.
[75] Khan F, Singh SN, Husain M. Effect of illumination intensity on cell parameters of a silicon solar cell. *Sol Energy Mater Sol Cells*, 2010, 94:1473–1476.
[76] Lim LHI, Ye Z, Ye J, *et al*. A linear method to extract diode model parameters of solar panels from a single I–V curve. *Renew Energy*, 2015, 76:135–142.